The 2022 Hormozgan doublet earthquakes: Two blind thrusts-related folding in Zagros fold-and-thrust belt, Southeast Iran

Ying-Hui Yang[1], Xiaoyun Li[1], Jyr-Ching Hu[2], Jiawei Song[1], Jingjin Zhao[3], Ali Yassaghi[4], Erwan Pathier[5], Qiang Xu[1], Qiang Chen[3]

1. State Key Laboratory of Geohazard Prevention and Geoenvironment Protection, Chengdu University of Technology, Chengdu, Sichuan, China
2. Department of Geosciences, National Taiwan University, Taipei, Taiwan, R.O.C.
3. Department of Remote Sensing and Geoinformation Engineering, Southwest Jiaotong University, Chengdu, Sichuan, China
4. Department of Geology, Tarbiat Modares University, Tehran, Iran
5. ISTerre, University Grenoble Alpes, CNRS, France

Key Points:

1. A doublet earthquakes event occurred in the southeastern of Zagros fold-and-thrust belt with a significant salt layers activity.
2. A higher dip angle and a shallower gentling blind faults are responsible for the 2022 Hormozgan doublet earthquakes.
3. The interseismic strain accumulation and salt diapir activity in the southeast of the seismic zone may cause this doublet earthquakes.

Abstract: A doublet earthquakes event including two main shocks with a magnitude larger than Mw 6.0 occurred on 1 July, 2022 in the Zagros fold-and-thrust belt, southeast Iran. The coseismic InSAR deformation field shows that this event caused significant surface uplift due to fault-related folding in the seismic zone. The estimated preferred faulting model suggests that a higher dip angle fault (maximum slip of ~1.1 m), and an overlying gentle dipping fault (maximum slip of ~1.2 m) within the Bandar-e-Lengeh Anticline, are responsible for the first and second main shocks, respectively. The calculated Coulomb failure stress change suggests that the first main shock has a significantly positive triggering effect in the second main shock. The coseismic deformation due to this doublet earthquakes is equal to the accumulated interseismic deformation for the past ~104 years. Finally, the salt diapir activity may affect the generation of the earthquake in the seismic zone.

1. Introduction

An earthquake with magnitude Mw 6.0 (first main shock) struck the provinces of Hormozgan and Fars, southern Iran, at 21:32 (UTC), on 1 July, 2022 (USGS, 2022a). After about two hours, a strong aftershock with magnitude of Mw 5.7 occurred at ~1.5 km southwest

of the first main shock (USGS, 2022b). Then, another strong earthquake with magnitude of Mw 6.0 (the second main shock) occurred at ~8.0 km southeast of the first main shock only two minutes after the Mw 5.7 aftershock (USGS, 2022c). These two main shocks caused non-negligible damage to the houses with low level of anti-seismic design, and at least 7 deaths, and ~49 injuries in the seismic zone.

This doublet earthquakes event occurred in the southeastern of Zagros fold-and thrust belt (Figs. 1 and S1). As a part of the Alpine-Himalayan orogenic system, the Zagros belt results from the oblique convergence and continental collision between the Arabian and Eurasian plates at the expense of the Neo-Tethys Ocean (Berberian & King, 1981; Agard et al., 2011; Lacombe et al., 2011). Both Zagros Folding and faulting, and salt layers govern the deformation in this part of the belt (Jahani et al., 2009; Hassanpour et al., 2021; Tavakolian et al., 2022). The belt also form front boundary of the oblique convergence (with rate of ~33 mm/yr) between the plates (Jackson, 1992; Talebian et al., 2002), and accommodated about half of the collision convergence rate between the two plates (Bachmanov et al., 2004; Hessami et al., 2006; Edwin et al., 2011). It caused the occurrence of thousands earthquakes in this zone each year, which caused the Zagros thrust-and-fold belt as one of the well-known areas with high seismic activity in the orogenic mountain belt (Penney et al., 2015; Golshadi et al., 2022). The 2022 Hormozgan earthquakes were the second doublet earthquakes event in the region, and the former event (the 2021 Fin doublet earthquakes) involved by two earthquakes with magnitudes of 6.0 and 6.4 (Figure 1), respectively. The Fin doublet earthquakes occurred in the nearby Fin town of Bandar Abbas city, ~100 km northeast of the 2022 Hormozgan doublet earthquakes, it has caused significant deaths, injuries and economic losses in this region (Nemati, 2022).

The reported focal mechanisms of the 2022 Hormozgan earthquakes by USGS (United States Geological Survey) and CGMT (Global Centroid Moment Tensor) shown that both of them were dominated by reverse motion. In addition, the seismic wave-derived focal mechanism suggests that these two main shocks have a similar fault attitude (Azimuth of strike and dip angle) (USGS, 2022a & 2022c). Therefore, whether these two main shocks occurred on one or two faults, was unknown to present. Furthermore, some active reverse faults including the Mountain Front Fault (MFF), and the Zagros Front Fault (ZFF) and the Bostaneh fault were close to the seismic zone (Figs. S2 and 5). Therefore, whether these faults were

reactivated by this doublet earthquakes is another key point of this study. Finally, the epicenters of the two main shocks are close to the Bandar-e-Lengeh Anticline, and it is likely that the rupture of the fault accommodated in this anticline is responsible for this doublet earthquakes event (Savidge et al., 2019; Yang et al., 2019b; Niazpour et al., 2021).

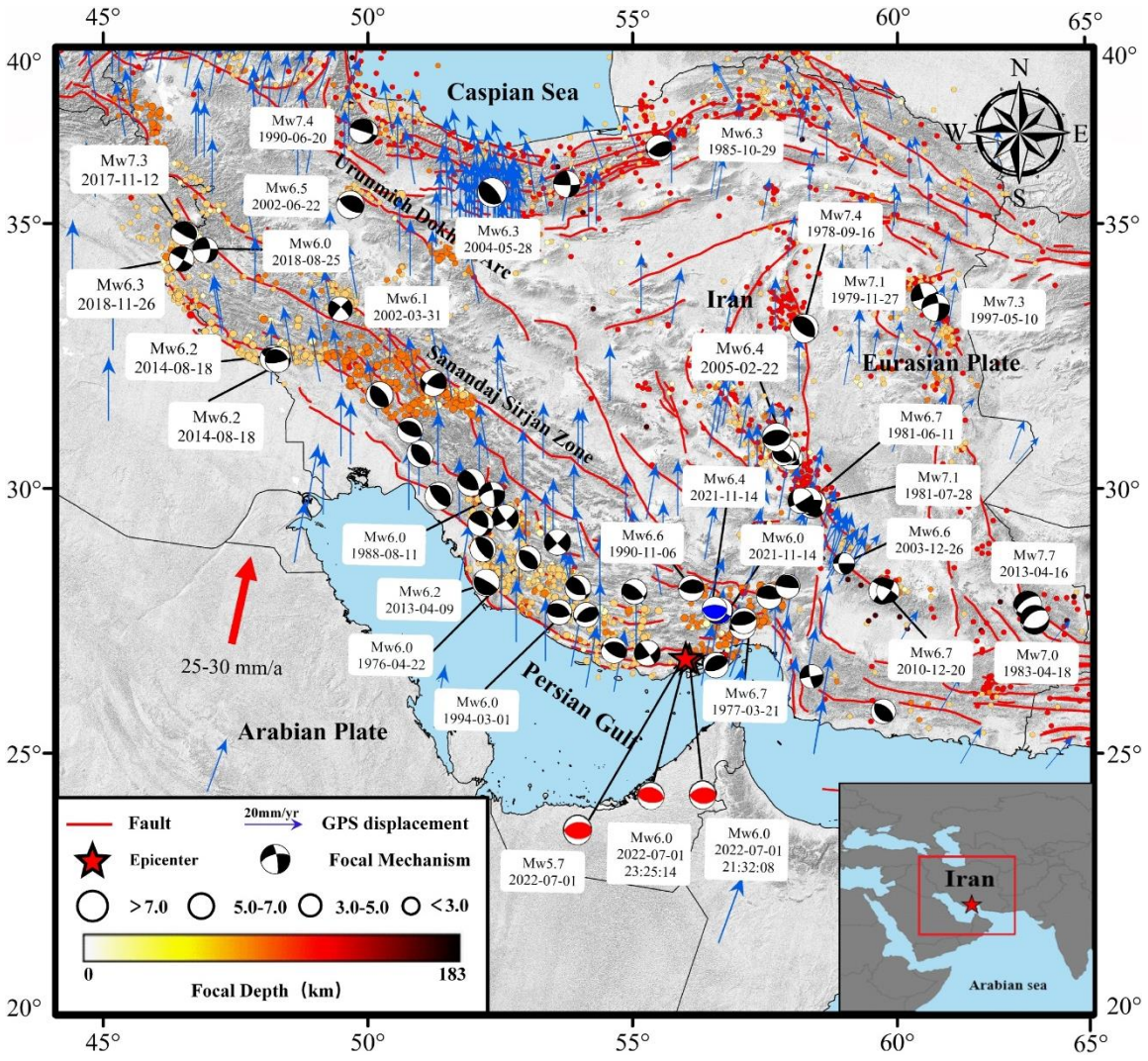

Figure 1 The tectonic background of southeast Iran. The red rectangle in insert shows the extent of the figure. The blue arrows denote the GPS horizontal displacement (Khorrami et al., 2019). The red solid lines indicate the active fault surface trace (Styron & Pagani, 2020), the circles are the historical earthquake (Karas özen et al., 2019), and the color of the circle gives the focal depth. The black beach balls show the mechanism of the historical earthquakes. The blue beach balls indicate the mechanism of 2021 Fin doublet earthquakes (Nemati, 2022). The red beach balls denote the mechanism of two main shocks and the largest aftershock with magnitude of Mw 5.7 (USGS, 2022a, 2022b & 2022c). The red star indicates the epicenter.

Here, the Synthetic Aperture Radar (SAR) images captured by Sentinel-1 satellite along ascending and the descending tracks were firstly used to measure the coseismic surface deformation fields of this doublet earthquakes. The source models of these two main shocks were estimated based on the coseismic InSAR observations. The seismic reflection profile and

model misfit were adopted to assess the reliability of the InSAR-derived faulting model. Then, the Coulomb failure stress change was used to reveal the triggering relation between these two main shocks. Finally, the interseismic surface deformation and salt diapir activity were discussed, to analyze the possible seismogenic mechanism of this doublet earthquakes event.

2. Datasets and Coseismic InSAR deformation

The 2022 Hormozgan earthquake sequence occurred in the southeastern Iran (USGS, 2022a, 2022b and 2022c). The sparse vegetal coverage and dry climate make it possible to extract the surface deformation based on the Sentinel-1A SAR images (See coverage in Fig. S2) with a short radar wavelength of ~ 5.5 cm (Yang et al., 2019a). Moreover, a short space and time baselines (Table S1) could decrease the negative effects caused by the DEM error and later aftershocks (Yang et al., 2018). It is worthy to note that the surface deformation caused by these two main shocks could not be separated due to their ~2 hours time interval, which is significantly shorter than the revisiting period of 12 days for the Sentinel-1A satellite.

The GAMMA software was adopted to carry out the 2-pass interference of the acquired SAR images (Wegmüller & Werner, 1997). The SRTM-V4 DEM was used to remove the topography phase component (Farr et al., 2007). The precise orbital data were used to calculate and remove the orbital phase component. The minimum cost flow algorithm was also used to unwrap the InSAR interferogram (Chen & Zebker, 2002). Then, a bilinear ramp was estimated using the far-field InSAR observations (Yang et al., 2018), and it was further removed from the unwrapped phase to weaken the orbital error. Moreover, the GACOS correction was introduced to mitigate the atmospheric delay phase component (Chen et al., 2021). Finally, the coseismic surface deformation of this doublet earthquakes was acquired and shown in Figure 2.

Significant surface displacement with maximum magnitude of ~0.32 m is observed mainly in the southwest side of the seismic zone (Figs. 2). Both the ascending and descending tracks InSAR deformation show a significant shortening motion along the satellite Light-Of-Sight (LOS) direction in the southwest of the seismic zone. Meanwhile, a slight negative InSAR deformation was found in the northeast of the seismic zone (Figs. 2). It suggests that the coseismic surface displacement is dominated by surface uplift motion, which is consistent with the reverse faulting mechanism derived by seismic wave data (USGS, 2022a and 2022c). Moreover, the significant InSAR deformation jumping across the Bandar-e-Lengeh anticline

(Fig. 2) indicates that a reverse fault dipping to southwest within this anticline may be responsible for the 2022 Hormozgan doublet earthquakes.

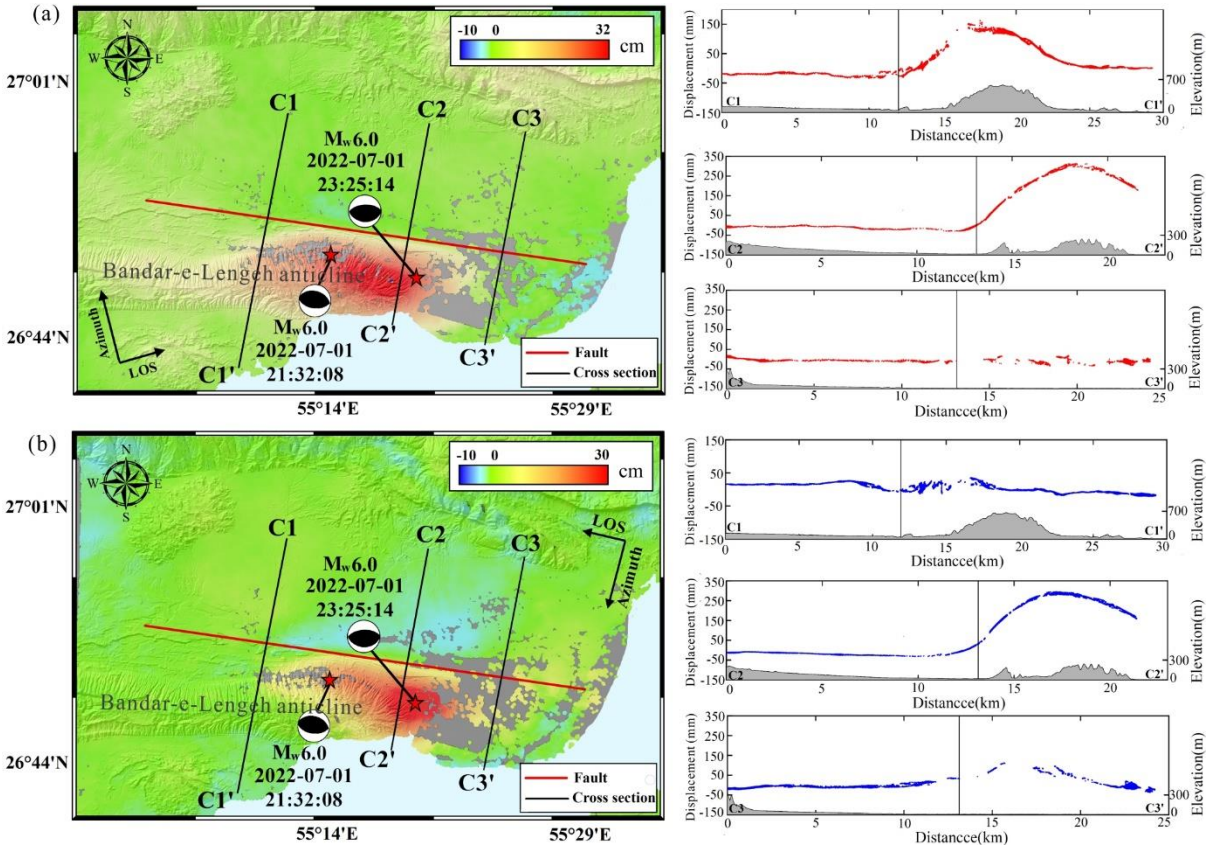

Figure 2 The coseismic InSAR deformation of the Sentinel-1 ascending (a) and descending (b) tracks of the 2022 Hormozgan doublet earthquakes. The red star denotes the epicenter. The black beach balls suggest the focal mechanism. The red solid line indicates the deformation boundary of positive and negative InSAR displacement. The black solid line indicates the three profiles. The coseismic surface displacement profiles are shown in the right panel.

3. Source model Methodology

Both the ascending and descending tracks InSAR observations were firstly masked, and the observations with low signal-to-noise ratio (interferometric coherence less than 0.3) were removed. Then, we applied the quadtree algorithm to under sample the InSAR data in order to decrease the computing load (Jonsson et al., 2002). Finally, 1389 and 1432 InSAR samples were kept for the ascending and descending tracks InSAR observations, respectively. These high signal-to-ratio InSAR samples were used for estimating the source model of the 2022 Hormozgan doublet earthquakes event.

Single fault model was firstly constructed to model the observed ascending and descending tracks InSAR observations. The fault length and width was set as 40 km×30 km

based on the InSAR deformation field. Considering the focal mechanism solutions of the USGS and GCMT, then, 94 °and [30 °, 150 °] was respectively set as initial value and searching range for the fault strike angle, 44 °and [0 °, 90 °] for the fault dip angle, -5 km and [-0.5km, 15 km] for the fault depth, 90 °and [0 °, 180 °] for the rake angle.

In addition, a rectangle dislocation within an elastic half-space model was adopted to calculate the surface displacement due to fault slip (Okada, 1985). And the fault plane was firstly divided into fault patches with a large size of 3.0 km×3.0 km (along the strike and down-dip directions). Then, the simulated annealing algorithm was used to search the best-fitting fault parameter under the constraint of the observed InSAR measurements. Finally, the searched best-fitting fault parameter was fixed, and then, the fault plane was divided using a small size of 1.0 km×1.0 km. The ununiform fault slip distribution was estimated using the least square method under the constraints of the InSAR observations.

In addition, a two faults model was also constructed to reveal the possible fault rupture pattern of this doublet earthquakes event. And the fault F1 (Fig. 2) located in the west of the F2 (the above-mentioned single fault), was added into the inversion processing. The fault length and width of F1 was given of 30 km×30 km. The initial fault strike angle of F1 was set as 90 ° (searching range [30 °, 150 °]) based on the ascending and descending tracks InSAR deformations and the published focal mechanism (USGS, 2022a). The other parameters including the fault dip angle, depth and rake angle were given the same initial value and searching range with the above-mentioned single fault.

4. Results and Discussions

4.1 A high dip angle fault and an overlying gentle dipping fault

Comparison of the fault parameters (including the single fault and two faults model) estimated in this study with others resources (Table S2) shows, that the parameters including the fault strike angle, dip angle of the two faults model, have a high consistency with the focal mechanism solution derived from seismic wave data (USGS, 2022a and 2022c). Meanwhile, the two faults model (Fig. 3) could accurately retrieve both the far- and near-filed InSAR deformations (Fig. 4), and some residuals in the far-field area (within the red dashed ellipse in Fig. 4b) could be due to the atmospheric delay noise and/or phase unwrapping error. However,

the residuals between the observed and predicted InSAR deformation by single fault model (Fig. S3), shows that there are non-negligible residuals in the near-fault area (within the black dashed ellipses in Fig. S4), especially for the satellite descending track InSAR observation.

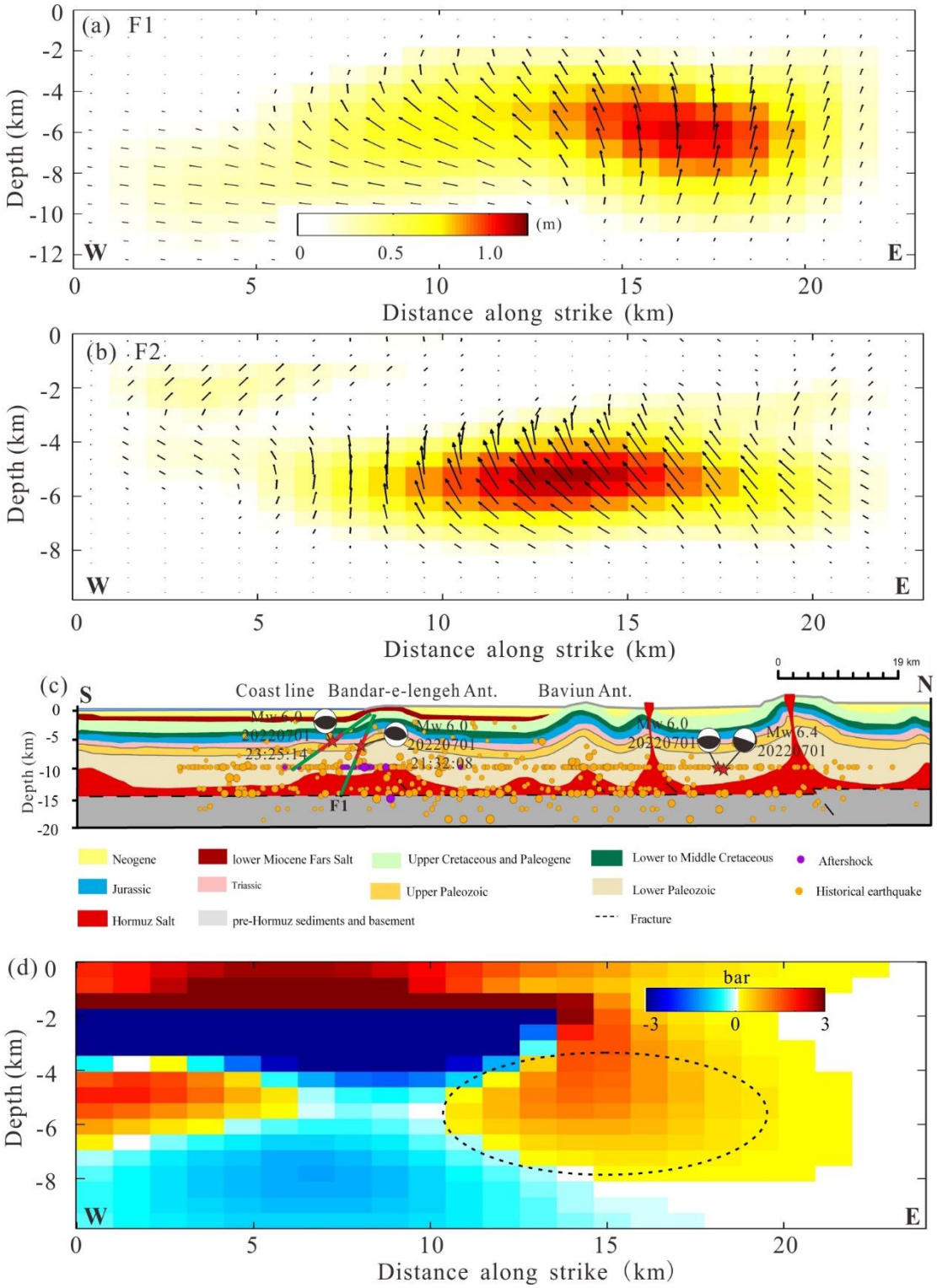

Figure 3 The InSAR-derived slip distribution of the first main shock (a, F1), and the second main shock (b, F2). (c) Interpreted seismic reflection profile along the S-N (Fig. S2, modified after Jahani et al., 2009). The green and red segments indicate the low slip and high slip area, respectively. The yellow circles indicate the

historical earthquake, and the grape circles denote the aftershocks. (d) Coulomb failure stress change on F2 due to the rupture of F1. The black dashed ellipse indicates the high-slip area of F2.

Furthermore, it is found that the ascending and descending tracks InSAR deformation misfits of the two faults model respectively decrease ~17%, ~28% than the results of single fault model. The higher consistency between the estimated fault parameters with the published results (USGS, 2022a & 2022c), and the smaller model misfit suggest that the two faults model should be the best-fitting solution of the 2022 Hormozgan doublet earthquakes. And the estimated seismic moment of the two faults are 2.68×10^{18} Nm (F1) and 2.75×10^{18} Nm (F2), equivalent to Mw 6.22 and Mw 6.23, respectively.

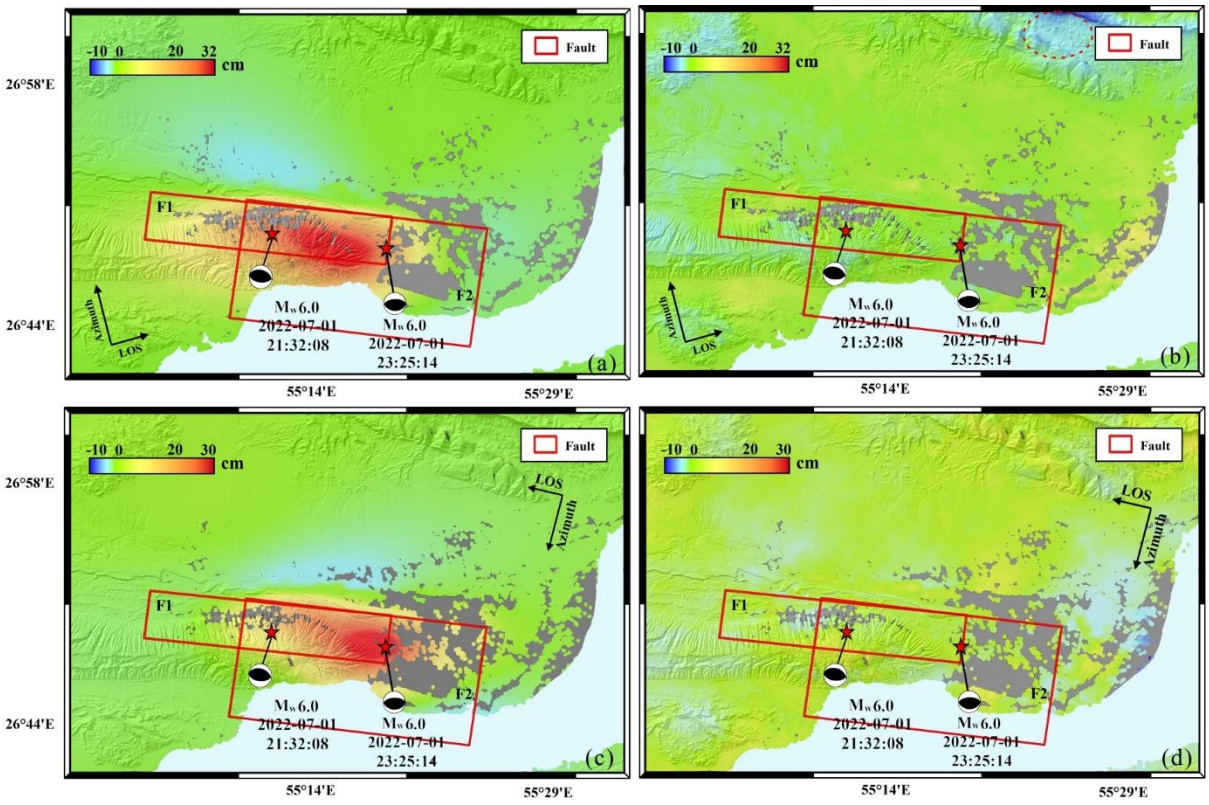

Figure 4 The predicted InSAR deformation of the satellite ascending (a) and descending (c) tracks based on estimated best-fitting faulting model (Fig. 3). (b) and (d) show the residual between the predicted and observed InSAR deformation for the satellite ascending and descending tracks, respectively. The red solid rectangles suggest the surface trace of the two seismogenic faults of F1 and F2. The red dashed ellipse denotes the significant deformation residual area. The red star indicates the epicenter, and the beach ball denotes the focal mechanism of two main shocks.

It could be found from Table S2 that the fault F1 has a high dip angle of 65.1 °, moreover, the rupture of F1 is controlled by a dominated reversing motion and slight strike-slip component, and the maximum slip magnitude on F1 is ~1.1 m, the slip asperity is located at the depths of 4.0-8.2 km under the ground surface (Figs. 3). Furthermore, Table S2 shows that

that the fault F1 has similar fault parameters with the published source mechanism of the first main shock (occurred on 21:32, Jul. 1, 2022). Therefore, it is hypothesized that the fault F1 should be the seismogenic fault of the first main shock of this doublet earthquakes event.

Furthermore, F2 has a gentler dip angle than F1 (with a dip angle of 33.1°), and the estimated faulting distribution (Fig. 3) shows that the significant slip on F2 is concentrated at depths of 4.0km-6.5km, which is slightly shallower than the depth of the high-slip area of F1. Moreover, the average reversing motion in the slip asperity of F2 is ~0.9 m, which is significantly larger than ~0.3 m of the average of the strike-slip component (Fig. 3). Table S2 shows that the fault parameters of F2 has a good consistency with the focal mechanism of the second main shock (USGS, 2022c). Therefore, the F2 should be the seismogenic fault of the second main shock. Finally, considering that there is no known fault in the seismic zone (Figs. 1 & S1) having similar fault parameters with the two estimated seismogenic faults, we propose that the thrust rupture on a blind higher dip angle fault (F1) and an overlying gentle dipping fault (F2) within the Bandar-e-Lengeh Anticline should be responsible for the 2022 Hormozgan doublet earthquakes.

4.2 The triggering relation between the two earthquakes

Only two hours interval between the two main shocks, indicates that the first main shock may has a triggering effect in the later one. Here, the Coulomb failure Stress Change (CSC) on the F2 caused by the fault slip of F1 was adopted to discuss the possible triggering relation between the two main shocks (Stein 1999; Harris, 2000; Huang et al., 2016). Figure 3d shows the calculated CSC on F2 by the rupture of F1, the receiver fault parameters were set as the same value with F2 (Table S2). It could be found from Figure 3d that the rupture of F1 significantly increased the Coulomb failure stress in the high-slip area of F2 (within the black dashed ellipse in Fig. 3d) with an average of ~0.7 bar, which is significant larger than the 0.1 bar threshold to trigger an earthquake (Harris, 2000).

The CSC distribution indicates that static Coulomb failure Stress transfer due to the first main shock has a non-negligible positive triggering effect in the second main shock. However, it is worthy to note that a large aftershock with a magnitude of Mw 5.7 (Figs. 1) occurred only 2 minutes before the second main shock (USGS, 2022b). Therefore, the dynamic Coulomb failure Stress caused by this large aftershock may also contribute to the seismogenic fault

rupture of the second main shock (Freed, 2005; Lay et al., 2010). A more comprehensive researches of both the static and dynamic CSC on F2 caused by previous earthquakes, could provide a better understanding on the triggering mechanism of this doublet earthquakes.

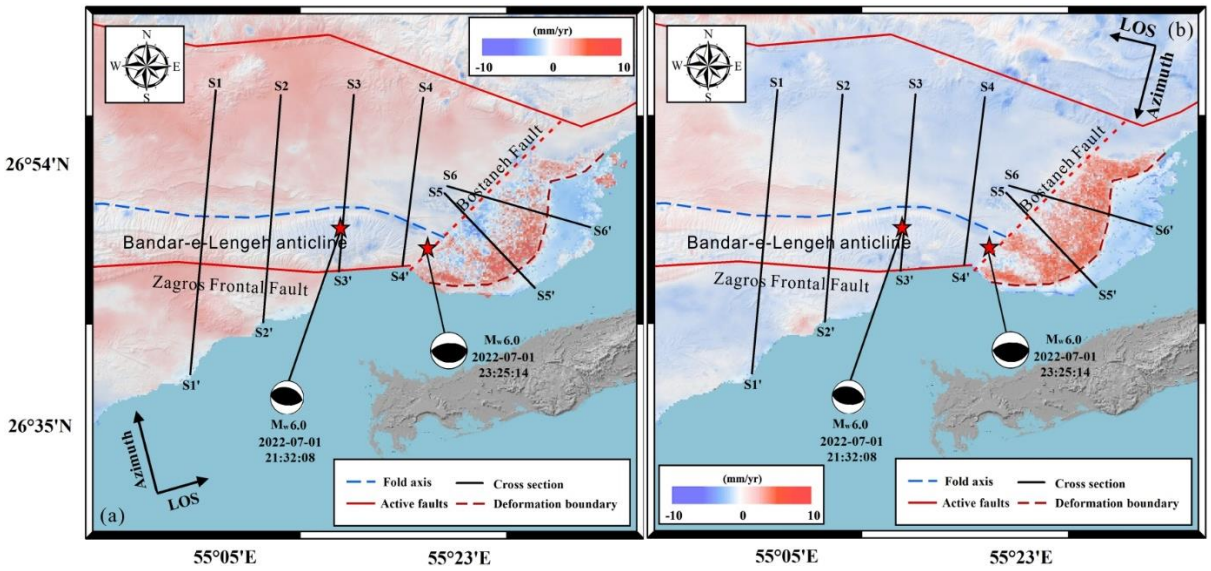

Figure 5 The interseismic InSAR deformation of the Sentinel-1 satellite ascending (a) and descending (b) tracks. The red star denotes the epicenter, and the beach balls indicate the focal mechanism of two main shocks. The black solid lines denote the surface trace of the deformation profiles (Fig. S5). The blue dashed lines indicate the surface trace of fault developed within the Bandar-e-Lengeh anticline. The red solid lines are the known active fault in this area. The red dashed line shows the boundary of abnormal uplift zone.

4.3 The interseismic tectonic motion in the seismic zone within salt diapir terrain

To investigate the interseismic tectonic motion in the seismic zone, the LICSBAS software was used to carry out the SBAS-InSAR processing based on the Sentinel-1 SAR images captured between May. 3, 2016 to Jan. 11, 2021 (Lazeck ý et al., 2020). Figure 5a (ascending track InSAR deformation) suggests that there is a significant deformation difference across the Bandar-e-Lengeh Anticline and the Zagros Frontal Fault. Meanwhile, it also could be found from Figure S5 that the interseismic deformation is affected by both the fault developed within the Bandar-e-Lengeh Anticline and the Zagros Frontal Fault. Furthermore, the average interseismic surface deformation is about -0.5 mm/yr in the seismic zone, however, it is ~2.0 mm/yr around the seismic zone (Fig. S5). It suggests that the interseismic surface deformation of the seismic zone is ~2.5 mm/yr relative to the surrounding area. The average satellite ascending track InSAR deformation (Fig. 2a) due to this doublet earthquakes event is ~0.26 m, if we assume that the coseismic surface deformation is releasing all the accumulated interseismic strain in this area, it would correspond to the total accumulated interseismic

deformation during the past ~104 years.

There is an abnormal InSAR deformation in the southeast area of the seismic zone (Fig. 5). Both the ascending and descending tracks InSAR observations suggest a significant shortening motion along the LOS direction. It is consistent with the vertical surface uplift motion that may be controlled by the uplift due to salt diapir activity. But we cannot exclude the InSAR bias caused by the phase misclosure (Ansari et al., 2021; Zheng et al., 2022). If we consider the salt diapir hypothesis, it can be noted that the surface uplift due to salt diapir activity (Fig. S1) has been widely found in the southeast part of Zagros (Jahani et al., 2009; Manea et al., 2021). Salt diapirs in this part of the Zagros are sourced the deep Hormuz Salt and the shallower lower Miocene Fars Salt (Fig. 3c) (Hassanpour et al., 2020). Therefore, it could be hypothesized that the found surface uplift in the southeast part of the seismic zone may also be caused by the diapir activities of the Hormuz and/or Fars salts. Meanwhile, the Bostaneh Fault (the red dashed line in Fig. 5) is the northwest boundary of this uplift area, and the possible reversing motion of the fault may also contribute to the found surface uplift. However, it is another challenge to reveal the mechanism of the found abnormal surface uplift. Moreover, more detailed researches needing to unravel whether the above-mentioned abnormal uplift has caused a significant influence on the 2022 Hormozgan doublet earthquakes.

5. Conclusion

The interseismic and coseismic InSAR deformations, seismic reflection profile and Coulomb failure stress are jointly used to reveal the mechanism of the 2022 Hormozgan doublet earthquakes. It is found that the rupture on a higher dip angle fault (F1) and an overlying gentle dipping fault (F2) within the Bandar-e-Lengeh Anticline associated with fault-related folding are responsible for the 2022 Hormozgan doublet earthquakes. In addition, the rupture of F1 significantly increases the Coulomb failure stress in the high-slip area of F2, it suggests that the first main shock may play an important role to trigger the second main shock. Meanwhile, it is found that this doublet earthquakes released ~104 years accumulated interseismic strain based on the interseismic and coseismic InSAR observations. Finally, the strong salt diapir activity in the southeast part of the seismic zone may also have an influence on the 2022 Hormozgan doublet earthquakes.

Acknowledgments

This research is supported by the Fund for Creative Research Groups of China (41521002), State Key Laboratory of Geohazard Prevention and Geoenvironment Protection Independent Research Project (SKLGP2021Z016), and Ministry of Science and Technology in Taiwan (110-2811-M-002-647 and 111-2811-M-002-116). And most figures are mapped based on the Generic Mapping Tools (GMT) software (Wessel & Smith, 1998).

Data Availability Statement

The Sentinel-1 SAR images could be freely acquired from the website of https://search.asf.alaska.edu/#/. The SRTM-DEM data is freely available from the website of http://srtm.csi.cgiar.org/. The GACOS data is freely available here: www.gacos.net. The produced data including the coseismic and interseismic InSAR deformations, the estimated faulting model and calculated Coulomb failure stress change data could be acquired on repository: https://doi.org/10.5281/zenodo.7041066.

References

[1] Agard, P., Omrani, J., Jolivet, L., Whitechurch, H., Vrielynck, B., Spakman, W., ... & Wortel, R. (2011). Zagros orogeny: a subduction-dominated process. *Geological Magazine*, 148(5-6), 692-725.

[2] Ansari, H., De Zan, F., & Parizzi, A. (2021). Study of systematic bias in measuring surface deformation with SAR interferometry. *IEEE Transactions on Geoscience and Remote Sensing*, 59(2), 1285-1301.

[3] Bachmanov, D., Trifonov, V., Hessami, K. T., Kozhurin, A., Ivanova, T., Rogozhin, E., et al. (2004). Active faults in the Zagros and central Iran. *Tectonophysics*, 380(3-4), 221-241.

[4] Berberian, M., & King, G. C. P. (1981). Towards a paleogeography and tectonic evolution of Iran. *Canadian Journal of Earth Sciences*, 18(2), 210-265. https://doi.org/10.1139/e81-019.

[5] Chen C. W., & Zebker, H. A. (2002). Phase unwrapping for large SAR interferograms: Statistical segmentation and generalized network models. *IEEE Transactions on Geoscience and Remote Sensing*, 40(8), 1709-1719. https://doi.org/10.1109/TGRS.2002.802453.

[6] Chen, Y. U., Li, Z., Bai, L., Muller, J. P., Zhang, J., & Zeng, Q. (2021). Successful Applications of Generic Atmospheric Correction Online Service for InSAR (GACOS) to the Reduction of Atmospheric Effects on InSAR Observations. *Journal of Geodesy and Geoinformation Science*, 4(1), 109. https://doi.org/10.11947/j.JGGS.2021.0113.

[7] Edwin N, Mohammad T, Jackson J A, et al. New views on earthquake faulting in the Zagros fold-and-thrust belt of Iran (2011). *Geophysical Journal International*, 186(3): 928-944.

[8] Farr, T. G., Rosen, P. A., Caro, E., Crippen, R., Duren, R., Hensley, S., ... & Alsdorf, D. (2007). The shuttle radar topography mission. *Reviews of Geophysics*, 45(2). https://doi.org/ 10.1029/2005RG000183.

[9] Freed, A. M. (2005). Earthquake triggering by static, dynamic, and postseismic stress transfer. *Annual Review of Earth and Planetary Sciences*, 33(1), 335-367.

[10] Golshadi, Z., Famiglietti, N. A., Atzori, S., & Vicari, A. (2022). Surface Displacement and Source Parameters of the 2021 Bandar-e Genaveh, Iran, Earthquake Determined from InSAR Observations.

303 *Applied Sciences*, 12(9), 4223. https://doi.org/10.3390/app12094223.
304 [11] Harris, R. A. (2000). Earthquake stress triggers, stress shadows, and seismic hazard. *Current Science*,
305 1215-1225.
306 [12] Hassanpour, J., Yassaghi, A., Muñoz, J. A., & Jahani, S. (2021). Salt tectonics in a double salt-source
307 layer setting (Eastern Persian Gulf, Iran): Insights from interpretation of seismic profiles and sequential
308 cross - section restoration. *Basin Research*, 33(1), 159-185.
309 [13] Hessami, K., Nilforoushan, F., & Talbot, C. J. (2006). Active deformation within the Zagros Mountains
310 deduced from GPS measurements. *Journal of the Geological Society*, 163(1), 143-148.
311 [14] Huang, M.-H., Tung H., Fielding, E., Huang, H.-H., Liang, C., Huang, C., & Hu, J.-C. (2016). Multiple
312 fault slip triggered above the 2016 Mw 6.4 MeiNong earthquake in Taiwan. *Geophysical Research*
313 *Letters*, 43, 7459-7467. https://doi.org/10.1002/2016GL069351.
314 [15] Jahani, S., Callot, J. P., Letouzey, J., & Frizon de Lamotte, D. (2009). The eastern termination of the
315 Zagros Fold-and-Thrust Belt, Iran: Structures, evolution, and relationships between salt plugs, folding,
316 and faulting. *Tectonics*, 28(6). https://doi.org/10.1029/2008TC002418.
317 [16] Jackson, J., (1992). Partitioning of strike-slip and covergent motion between Eurasia and Arabia in
318 eastern Turkey and the Caucasus. *Journal of Geophysical Research: Solid Earth*, 97, 12471-12479.
319 [17] Jonsson, S., Zebker, H., Segall, P. & Amelung, F. (2002). Fault slip distribution of the 1999 Mw 7.1
320 Hector Mine, California, Earthquake, estimated from satellite radar and GNSS measurements. *Bulletin*
321 *of the Seismological Society of America*, 92(4), 1377-1389.
322 [18] Karasözen, E., Nissen, E., Bergman, E. A., & Ghods, A. (2019). Seismotectonics of the Zagros (Iran)
323 from orogen - wide, calibrated earthquake relocations. *Journal of Geophysical Research: Solid Earth*,
324 124(8), 9109-9129.
325 [19] Khorrami, F., Vernant, P., Masson, F., Nilfouroushan, F., Mousavi, Z., Nankali, H., ... & Alijanzade, M.
326 (2019). An up-to-date crustal deformation map of Iran using integrated campaign-mode and permanent
327 GPS velocities. *Geophysical Journal International*, 217(2), 832-843.
328 [20] Lay, T., Ammon, C. J., Kanamori, H., Rivera, L., Koper, K. D., & Hutko, A. R. (2010). The 2009
329 Samoa–Tonga great earthquake triggered doublet. *Nature*, 466(7309), 964-968.
330 https://doi.org/10.1038/nature09214.
331 [21] Lacombe, O., Grasemann, B., & Simpson, G. (2011). Introduction: geodynamic evolution of the Zagros.
332 *Geological Magazine*, 148(5-6), 689-691. https://doi.org/10.1017/S001675681100046X.
333 [22] Lazecký, M., Spaans, K., González, P. J., Maghsoudi, Y., Morishita, Y., Albino, F., ... & Wright, T. J.
334 (2020). LiCSAR: An automatic InSAR tool for measuring and monitoring tectonic and volcanic activity.
335 *Remote Sensing*, 12(15), 2430.
336 [23] Manea, V. C., Armaş, I., Manea, M., & Gheorghe, M. (2021). InSAR surface deformation and numeric
337 modeling unravel an active salt diapir in southern Romania. *Scientific Reports*, 11(1), 1-9.
338 https://doi.org/10.1038/s41598-021-91517-4.
339 [24] Nemati, M. (2022). The November 2021 Fin (SE Zagros, Iran) doublet earthquakes of reverse faults in
340 a transpressional tectonic regime. https://doi.org/10.21203/rs.3.rs-1314781/v1.
341 [25] Niazpour, B., Shomali, Z. H., & Cesca, S. (2021). Source study of 2017 Hojedk triplet earthquake
342 sequence, southeast Iran. *Journal of Seismology*, 25(1), 85-101. https://doi.org/10.1007/s10950-020-
343 09934-3.
344 [26] Okada, Y. (1985). Surface deformation due to shear and tensile faults in a half-space. *Bulletin of the*
345 *Seismological Society of America*, 75(4), 1135-1154.
346 [27] Penney, C., Copley, A., & Oveisi, B. (2015). Subduction tractions and vertical axis rotations in the

Zagros-Makran transition zone, SE Iran: The 2013 May 11 Mw6.1 Minab earthquake. *Geophysical Journal International*, 202(2), 1122-1136. https://doi.org/10.1093/gji/ggv202.

[28] Savidge, E., Nissen, E., Nemati, M., Karasözen, E., Hollingsworth, J., Talebian, M., ... & Rashidi, A. (2019). The December 2017 Hojedk (Iran) earthquake triplet-sequential rupture of shallow reverse faults in a strike-slip restraining bend. *Geophysical Journal International*, 217(2), 909-925. https://doi.org/10.1093/gji/ggz053.

[29] Stein, R. S. (1999). The role of stress transfer in earthquake occurrence. *Nature*, 402(6762), 605-609.

[30] Styron, R., & Pagani, M. (2020). The GEM global active faults database. *Earthquake Spectra*, 36(1_suppl), 160-180.

[31] Talebian M., Jackson J. (2002). Offset on the Main Recent Fault of NW Iran and implications for the late Cenozoic tectonics of the Arabia-Eurasia collision zone. *Geophysical Journal International*, 150.

[32] Tavakolian, I., Yassaghi, A., & Najafi, M. (2022). Structural Style in the South Dezful Embayment, SW Iran: Combined Influence of the Zagros Frontal Fault System and the Detachment in the Miocene Gachsaran Formation. *Journal of Petroleum Geology*, 45(3), 303-323.

[33] United States Geological Survey (USGS), 2022a. M6.0-55km NE of Bandar-e Lengeh, Iran. https://earthquake.usgs.gov/earthquakes/eventpage/us6000hz8x/executive.

[34] United States Geological Survey (USGS), 2022b. M5.7-54km NE of Bandar-e Lengeh, Iran. https://earthquake.usgs.gov/earthquakes/eventpage/us6000hz9p/executive.

[35] United States Geological Survey (USGS), 2022c. M6.0-56km NE of Bandar-e Lengeh, Iran. https://earthquake.usgs.gov/earthquakes/eventpage/us6000hz9v/executive.

[36] Wegmüller, U., & Werner, C. (1997). Gamma SAR processor and interferometry software. *ESA SP* (Print), 1687-1692.

[37] Wessel, P., & Smith, W. H. (1998). New, improved version of Generic Mapping Tools released. *Eos, Transactions American Geophysical Union*, 79(47), 579-579.

[38] Yang Y. H., Tsai M. C., Hu J. C., et al., (2018). Coseismic slip deficit of the 2017 Mw 6.5 Ormoc Earthquake that occurred along a creeping segment and geothermal field of the Philippine Fault. *Geophysical Research Letter*. 45(6), 2659-2668. https://doi.org/10.1002/2017GL076417.

[39] Yang Y. H., Hu J. C., Ali Y., et al., (2019a). Midcrustal Thrusting and Vertical Deformation Partitioning Constraint by 2017 Mw 7.3 Sarpol Zahab Earthquake in Zagros Mountain Belt, Iran. *Seismological Research Letter*. 89(6), 2204-2213. https://doi.org/10.1785/0220180022.

[40] Yang, Y. H., Hu, J. C., Chen, Q., Wang, Z. G., & Tsai, M. C. (2019b). A Blind Thrust and Overlying Folding Earthquake of the 2016 Mw 6.0 Hutubi Earthquake in the Northern Tien Shan Fold-and-Thrust Belts, China. *Bulletin of the Seismological Society of America*, 109(2), 770-779. https://doi.org/10.1785/0120180150.

[41] Zheng, Y., Fattahi, H., Agram, P., Simons, M., & Rosen, P. (2022). On Closure Phase and Systematic Bias in Multilooked SAR Interferometry. *IEEE Transactions on Geoscience and Remote Sensing*, 60, 1-11.